JACS
JOURNAL OF THE AMERICAN CHEMICAL SOCIETY
pubs.acs.org/JACS

Article

Photochemical Formation and Electronic Structure of an Alkane σ-Complex from Time-Resolved Optical and X-ray Absorption Spectroscopy

Raphael M. Jay,* Michael R. Coates, Huan Zhao, Marc-Oliver Winghart, Peng Han, Ru-Pan Wang, Jessica Harich, Ambar Banerjee, Hampus Wikmark, Mattis Fondell, Erik T. J. Nibbering, Michael Odelius,* Nils Huse,* and Philippe Wernet*

Cite This: J. Am. Chem. Soc. 2024, 146, 14000−14011

Read Online

ACCESS | Metrics & More | Article Recommendations | Supporting Information

ABSTRACT: C−H bond activation reactions with transition metals typically proceed via the formation of alkane σ-complexes, where an alkane C−H σ-bond binds to the metal. Due to the weak nature of metal−alkane bonds, σ-complexes are challenging to characterize experimentally. Here, we establish the complete pathways of photochemical formation of the model σ-complex $Cr(CO)_5$-alkane from $Cr(CO)_6$ in octane solution and characterize the nature of its metal−ligand bonding interactions. Using femtosecond optical absorption spectroscopy, we find photoinduced CO dissociation from $Cr(CO)_6$ to occur within the 100 fs time resolution of the experiment. Rapid geminate recombination by a fraction of molecules is found to occur with a time constant of 150 fs. The formation of bare $Cr(CO)_5$ in its singlet ground state is followed by complexation of an octane molecule from solution with a time constant of 8.2 ps. Picosecond X-ray absorption spectroscopy at the Cr L-edge and O K-edge provides unique information on the electronic structure of the $Cr(CO)_5$-alkane σ-complex from both the metal and ligand perspectives. Based on clear experimental observables, we find substantial destabilization of the lowest unoccupied molecular orbital upon coordination of the C−H bond to the undercoordinated Cr center in the $Cr(CO)_5$-alkane σ-complex, and we define this as a general, orbital-based descriptor of the metal−alkane bond. Our study demonstrates the value of combining optical and X-ray spectroscopic methods as complementary tools to study the stability and reactivity of alkane σ-complexes in their role as the decisive intermediates in C−H bond activation reactions.

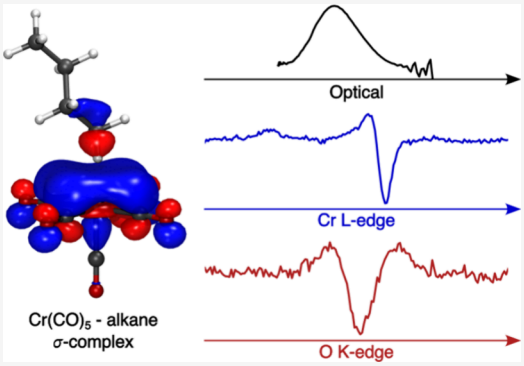

INTRODUCTION

Alkane σ-complexes play a critical role in C−H bond activation reactions with transition metal complexes. They constitute the decisive intermediates in which an alkane C−H bond directly coordinates and interacts with the transition metal.[1−3] Due to their low polarizability, however, alkanes are generally poor electron donors and acceptors. The bond strength between the metal and the alkane C−H bond in σ-complexes is therefore typically very weak. Still, the subtle degree of polarization induced in the C−H bond through binding to the metal site in σ-complex intermediates critically determines the reactivity toward bond cleavage in C−H activation reactions.[4] In pursuit of understanding this unusual bonding configuration, a rich literature of complexes, in which alkane C−H bonds act as ligands bound to a metal center, has emerged over the decades.[3,5−7]

Various routes exist toward preparation of alkane σ-complexes. Direct preparation in the solid state has been achieved by hydrogenation of metal-bound alkenes[8,9] as well as in solution via protonation of a metal-bound alkyl group at very low temperature.[10] The most common routes to preparing alkane σ-complexes, however, are photochemical ones[3] (see Scheme 1). The photoinduced elimination of a ligand from certain transition metal complexes leads to the creation of an

Scheme 1. Reaction Scheme of Photochemical Alkane σ-Complex Formation

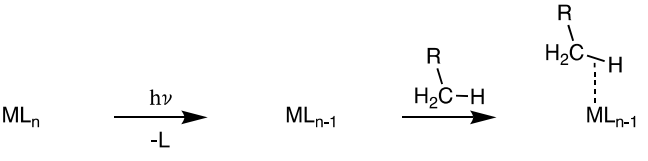

Received: February 9, 2024
Revised: April 29, 2024
Accepted: April 30, 2024
Published: May 7, 2024

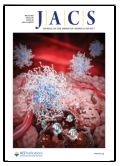

undercoordinated and highly reactive species capable of binding an alkane from solution. This type of photochemical preparation has been the basis for a wide range of spectroscopic investigations of alkane σ-complexes. Early flash photolysis experiments in low-temperature matrices as well as solution unambiguously established that alkanes can indeed act as ligands in a metal complex.[11−14] Later, nuclear magnetic resonance (NMR) and time-resolved infrared (IR) spectroscopy, in particular, were instrumental in characterizing the structure of alkane σ-complexes as well as their mechanistic role in C−H activation reactions.[15−22]

As the precursor to $Cr(CO)_5$-alkane, one of the first ever observed alkane σ-complexes,[11,13,14] chromium hexacarbonyl ($Cr(CO)_6$), has long served as a model systems for both developing a general mechanistic understanding of photoinduced ligand exchange and gaining specific insight into the nature and properties of alkane σ-complexes.[6] However, while constituting a thoroughly studied model system, experimentally resolving the ultrafast time scales of the formation of $Cr(CO)_5$-alkane σ-complexes has proven difficult. NMR spectroscopy is intrinsically slow compared to ligand-exchange dynamics and can only probe species that are metastable on nano- to millisecond time scales. Time-resolved IR spectroscopy accesses the time scales necessary to detect σ-complexes but has limited sensitivity to their electronic structure and to the sub-picosecond regime of excited-state and dissociation dynamics due to the broad and overlapping IR absorption bands of vibrationally hot species on these time scales.

Here, we combine femtosecond optical absorption and picosecond X-ray absorption spectroscopy[23,24] to determine, based on the complementary time scales and properties these methods access, the photochemical pathway of formation and the bonding characteristics of σ-complexes with $Cr(CO)_6$ in alkane solution. Femtosecond optical absorption spectroscopy has been used before to follow the initial steps in the ligand-exchange dynamics of $Cr(CO)_6$ and other transition metal complexes in various solvents including alkanes.[25−32] Due to insufficient time resolution and detection sensitivity, however, these investigations were unable to robustly resolve and assign the intermediates along the alkane σ-complex formation from $Cr(CO)_6$ observed on the femtosecond time scale.[25,30] To date, the pathway of photochemical formation of $Cr(CO)_5$-alkane and many other σ-complexes has not been fully resolved. For instance, it has remained unclear what the time scale of CO dissociation in solution is, whether CO dissociation produces a bare $Cr(CO)_5$ fragment in solution before binding to an alkane, and, if so, whether $Cr(CO)_5$ is present in its ground or an excited state. Answering these questions is critical for developing a fundamental mechanistic understanding of ligand-exchange reactions as the basis for alkane σ-complex formation in photochemical C−H activation reactions with transition metals.

Time-resolved X-ray absorption spectroscopy has previously been shown to provide information highly complementary to the information provided by time-resolved optical and infrared absorption spectroscopy. Measuring the extended absorption fine structure (EXAFS) at the tungsten L-edge has recently allowed Bartlett et al. to determine metal−alkane bond lengths in $W(CO)_5$-alkane σ-complexes.[33] By evaluating the character of main-edge transitions in the rhodium L-edge absorption spectrum, the metal−alkane orbital interactions upon formation of rhodium−alkane σ-complexes as well as the ensuing C−H bond cleavage via oxidative addition have recently been observed.[34] The direct access of X-ray absorption spectroscopy to the relevant metal d-derived orbitals by the 2p → nd transitions underlying transition metal L-edges allows evaluating the degree to which metal d orbitals hybridize with incoming alkane C−H bonds. Such properties of alkane σ-complexes, which have thus far mostly been studied using theory,[35−38] can now be validated experimentally.[34] Here, we use the respective capabilities of femtosecond optical absorption and picosecond X-ray absorption spectroscopy to unambiguously establish the full photochemical pathways of $Cr(CO)_6$ dissociation in octane solution and to characterize the electronic structure of the resulting $Cr(CO)_5$-alkane σ-complex within novel orbital-based descriptors.

METHODS

Materials. $Cr(CO)_6$ was prepared in *n*-octane (purchased from Sigma-Aldrich) at concentrations of 7 mM for the time-resolved transient optical and 20 mM for the X-ray absorption measurements. To achieve the concentration of the X-ray absorption measurements, the sample was stirred and put into a sonication bath for up to ∼1 h.

Transient UV−Visible Absorption Spectroscopy. Time-resolved UV−visible measurements were conducted using a 3 kHz Ti:sapphire amplified laser system (Spectra Physics Spitfire Ace, 90 fs, 800 nm). The sample was prepared as a free-flowing 300 μm thick wire-guided liquid sheet. The sample was optically excited by the third harmonic of the fundamental laser wavelength with a fluence of 4.6 mJ/cm^2. A supercontinuum pulse (generated in a 1 mm calcium fluoride plate) was used to probe the absorbance change in transmission using a prism-based imaging spectrograph and a CCD detector, while a second supercontinuum pulse served as a reference. The data were chirp-corrected by using the delay at half-rise of the signal onset for every wavelength. The time resolution as determined by the rise time of the transient absorption signals was ∼100 fs. Pump−probe measurements of the pure octane solvent under the same experimental conditions showed a negligible contribution of a coherent artifact to the pump-induced signal around zero delay.

Time-Resolved X-ray Absorption Spectroscopy. The time-resolved X-ray absorption measurements were performed at the UE52-SGM beamline[39] of the BESSY II synchrotron. The X-ray absorption data were acquired in transmission geometry using a flatjet sample delivery system.[40,41] The liquid sample was transported into the experimental vacuum chamber via two colliding jets, thereby forming a thin liquid sheet. To form a stable octane sheet, flow rates were kept between 4.5 and 5 mL/min using a pair of nozzles with a diameter of ∼50 μm. The thickness of the liquid sheet was between 4.3 and 4.6 μm throughout all measurements as estimated from the comparison of the transmissions at 528 eV (O K-edge) and 573 eV (Cr L-edge) to tabulated values.[42] The bandwidth of the incidence X-rays was ∼200 meV at the O K-edge and ∼250 meV at the Cr L-edge. The sample was optically excited by the fourth harmonic of a fiber laser (Amplitude Tangerine, 1030 nm, 350 fs) at 258 nm wavelength. The repetition rate of the laser was set to 208 kHz for all measurements. The laser pulse energy was ∼5 μJ at a spot size of ∼60 × 100 μm^2 at the sample, amounting to an overall laser fluence of ∼100 mJ/cm^2. The time resolution as derived from the rise time of the transient X-ray signals was ∼45 ps (determined by the X-ray pulse duration).

Computational Details. Geometry optimizations were performed with the Gaussian 16 quantum chemistry suite[43] on the level of density functional theory (DFT) using the TPSSh functional[44,45] and the def2-TZVP[46,47] basis set. $Cr(CO)_6$ was optimized in O_h symmetry, $Cr(CO)_5$ in both C_{4v} and C_{2v} symmetry, and $Cr(CO)_5$-butane in C_1 symmetry. The butane-based σ-complex was used instead of the octane-based σ-complex to reduce the computational cost. Solvent effects were incorporated in the geometry optimizations by implicit solvation given by the conductor-like polarizable continuum model (CPCM)[48,49] using a dielectric constant corresponding to octane (ε = 1.9406). Based on these structures, the

https://doi.org/10.1021/jacs.4c02077
J. Am. Chem. Soc. 2024, 146, 14000−14011

Cr L-edge spectra were simulated using the restricted active space self-consistent field[50] (RASSCF) wave function, while the optical and O K-edge spectra were simulated using time-dependent density functional theory (TD-DFT). The details of each method are described below.

The RASSCF Cr L-edge absorption spectra were simulated in OpenMolcas.[51] For all spectra, the active space was constructed by rotating the Cr 2p orbitals (frozen at the Hartree−Fock level) into the RAS1 subspace and allowing at most 1 hole in the RAS1 subspace, rotating occupied valence orbitals in RAS2 and low-lying virtual orbitals in RAS3, allowing for at most 2 electrons in the RAS3 subspace. Starting with $Cr(CO)_6$, 16 electrons are distributed in 19 orbitals corresponding to the $1t_{1u}$ (2p) core orbitals, $5e_g$ (σ CO-$d_{x^2-y^2}$ and σ CO-d_{z^2}) and $2t_{2g}$ (d-π CO*) occupied orbitals, and the $9t_{1u}$ (π CO*), $2t_{2u}$ (π CO*), $3t_{2g}$ (π CO*-d), and $6e_g$ ($d_{x^2-y^2}$-σ CO and d_{z^2}-σ CO) unoccupied orbitals, resulting in a wave function denoted RAS(16,1,2;3,5,11). For the RASSCF L-edge spectra, zeroth-order relativistic effects were incorporated by the Douglas−Kroll−Hess Hamiltonian[52] for the ANO-RCC-VTZP basis set[53,54] used for all atoms. Eighty singlet and 80 triplet valence states were independently solved for by a state-averaged RASSCF wave function. A total of 240 singlet and 480 triplet core-excited states were independently solved for by a state-averaged RASSCF wave function by using the HEXS keyword in the RASSCF module in OpenMolcas. The subsequent spin−orbit coupled L-edge spectra were obtained by the RASSI module.[55] All other complexes ($Cr(CO)_5$ (C_{4v}), $Cr(CO)_5$ (C_{2v}), and $Cr(CO)_5$-butane) employed the same active space allowing for changes in orbital character. All spectrum calculations were performed in C_1 symmetry.

TD-DFT calculations of the optical and O K-edge absorption spectra were performed using the ORCA quantum chemistry package[56,57] at the B3LYP level of theory[58,59] with the def2-TZVP basis set.[46,47] For computational efficiency, the RIJCOSX approximation[60] was used. For the optical absorption spectra, 30 roots were calculated. For the O K-edge absorption spectra, the Pipek−Mezey orbital localization scheme[61] was used, and the excitation window was restricted to only include the O 1s orbitals. The number of calculated roots was set to 30 roots per O atom for the different species.

The simulated optical absorption spectra were generated by convolving the calculated transitions with a Gaussian function with a width of 0.3 eV full width at half-maximum (fwhm) to account for the experimental and inhomogeneous broadening. The simulated X-ray absorption spectra were generated by convolving the calculated transitions with a pseudo-Voigt function. The Lorentz contribution to the Voigt function accounts for the tabulated lifetime broadening[62] of 0.32 eV fwhm at the Cr L_3-edge, 0.76 eV at the Cr L_2-edge, and 0.18 eV at the O K-edge. The Gaussian contribution of 0.4 eV fwhm throughout the Cr L-edge and 0.8 eV at the O K-edge accounts for the experimental and inhomogeneous broadening. To align the calculated spectra with the experimental spectra, a uniform shift of −6.47 eV was applied at the Cr L-edge, whereas a shift of +13.7 eV was applied at the O K-edge. This is done to compensate for errors accumulated from the approximations used in simulating the X-ray absorption spectra. The relative shifts between each species are therefore preserved within each method used.

RESULTS AND DISCUSSION

Transient UV−Visible Absorption Spectroscopy. Figure 1a shows an overview of the transient optical absorption data of $Cr(CO)_6$ in octane solution covering pump−probe delays up to 300 ps. Representative cuts along the spectral range are displayed in Figure 1b for selected pump−probe delays. The inset in Figure 1b shows negligible steady-state absorption of $Cr(CO)_6$ in the spectral range probed in the transient absorption measurements. The time-resolved data qualitatively reproduce earlier transient absorption data of $Cr(CO)_6$ and other metal hexacarbonyl complexes in various solvents including alkanes.[25,29,30] With improved detection sensitivity and temporal resolution, our measurements now reveal new information. Within the time resolution of the experiment, a broad absorption appears, which stretches across the observed spectral range at the earliest measured time delays and which decreases in spectral bandwidth within the first few hundred femtoseconds. At the same time, a strong absorption band can be observed for wavelengths shorter than 450 nm (Figure 1a). Additionally, oscillatory signals are apparent at delay times below 2 ps in the spectral range between 600 and 720 nm (oscillatory signals are faintly visible below 450 nm as well, as detailed below). Within a few picoseconds, we see a broad transient absorption band emerging in the red part of the spectrum and gradually moving to shorter wavelengths concomitant with the decay of the absorption below 450 nm (Figure 1a). An additional blue-shift as well as a narrowing of the absorption band around 500 nm takes place on the time scale of tens to hundreds of picoseconds (Figure 1b). This prominent absorption band was previously observed and identified as a transition between the highest occupied molecular orbital (HOMO) and the lowest unoccupied molecular orbital (LUMO) of the solvent-complexed $Cr(CO)_5$ fragment in its electronic ground state.[13] Notably, the energy of this transition was shown to scale with the bond strength toward the associated molecule,[11,14] and we will use this property later in our analysis.

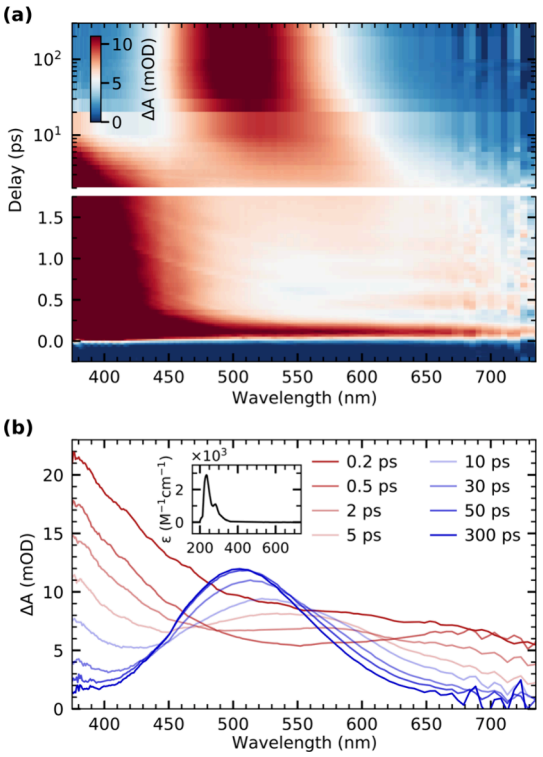

Figure 1. (a) Overview of the transient optical absorption data of $Cr(CO)_6$ in octane solution following photoexcitation with a 266 nm laser pulse. (b) Transient absorption spectra for selected pump−probe delays displaying an initial broad absorption feature throughout the observed spectral range followed by formation of a transient absorption band centered at around 500 nm. The steady-state absorption spectrum of $Cr(CO)_6$ is shown in the inset.

Cuts along the pump−probe delay axis for selected wavelengths are displayed in Figure 2a for closer inspection. The three delay traces are modeled by a global fit based on a biexponential model, yielding a fast time constant of 150 ± 10

https://doi.org/10.1021/jacs.4c02077
J. Am. Chem. Soc. 2024, 146, 14000−14011

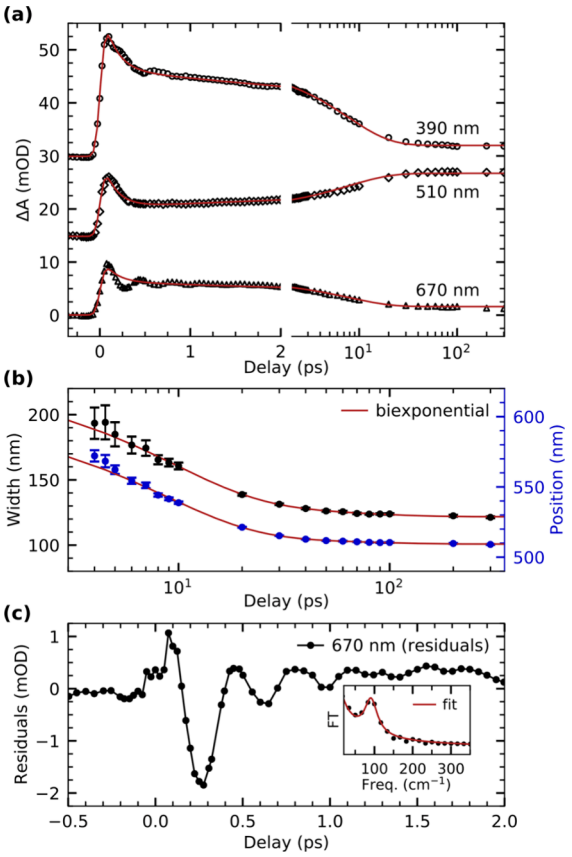

Figure 2. (a) Delay traces extracted at three different wavelengths and modeled with a global fit based on a biexponential model. (b) Width and position of the transient absorption band arising after photoexcitation in the range of 480 to 640 nm as a function of pump−probe delay. The evolution of both width and position is modeled by a biexponential function. (c) Residuals of the global fit of the delay trace at 670 nm from panel (a) with a Fourier transfer (FT) analysis of the residuals depicted in the inset. The fit is the sum of a Lorentzian line shape and, to account for the background, the inverse frequency ν, a/ν, where a is a fit parameter.

fs and a slower time constant of 7.7 ± 0.3 ps. The first time constant of 150 fs, which describes the initial decrease of the broad absorption across the observed spectral range, quantitatively reproduces dynamics reported in earlier femtosecond IR measurements,[63] where the recovery of the bleach signal on the same time scale was assigned to geminate recombination of dissociated CO with the $Cr(CO)_5$ fragment. The second time constant of 7.7 ps we instead assign to the association of an octane molecule from solution in agreement with previous femtosecond studies on $Cr(CO)_6$ as well as other metal carbonyls.[29,30,32,34]

The results of the analysis of the width and position of this HOMO → LUMO absorption band are shown in Figure 2b (see Supporting Information for details of the analysis). The evolution of both width and position is well described by a biexponential temporal behavior, where the fast component of 8.6 ± 0.6 ps is in good agreement with the time scale of 7.7 ± 0.3 ps determined from the global fit of the delay traces in Figure 2a and assigned to σ-complex formation. Given that the two values stem from independent observables, we define the mean of 8.2 ± 0.4 ps as the time constant for σ-complex formation. The slower time constant of 53 ± 12 ps of the biexponential fit is assigned to thermalization of the σ-complex with the solvent environment, in agreement with previous measurements of other metal carbonyls in solution.[29,30,64] We find the final peak position of the $Cr(CO)_5$-alkane σ-complex after ∼100 ps to be at 510 nm. This wavelength is in excellent agreement with the band position of $Cr(CO)_5$ bound to an alkane in solution and in noble gas matrices as derived from flash photolysis measurements.[12−14]

The oscillatory signal observed right after the UV excitation in the red part of the overview map in Figure 1a can be isolated by evaluating the residuals from the fit of the delay trace at 670 nm displayed in Figure 2c. A Fourier analysis of these data (shown in the inset) reveals a single frequency of 91 ± 1 cm^{-1}. This is in good agreement with the coherent oscillations observed in the photochemistry of gas-phase $Cr(CO)_6$.[65−67] In the gas phase, these oscillations have been assigned to equatorial Cr-CO bending modes in the S_0 ground state of $Cr(CO)_5$ with C_{4v} symmetry. These modes are thought to be populated following the passing of the S_1 excited state of $Cr(CO)_5$, which exhibits D_{3h} symmetry[65−68] (see Scheme 2).

Scheme 2. Schematic Depiction of the Potential Energy Surfaces along Photoinduced CO Dissociation from $Cr(CO)_6$ and Subsequent Formation of the $Cr(CO)_5$ Fragment (Adapted from Ref 68)

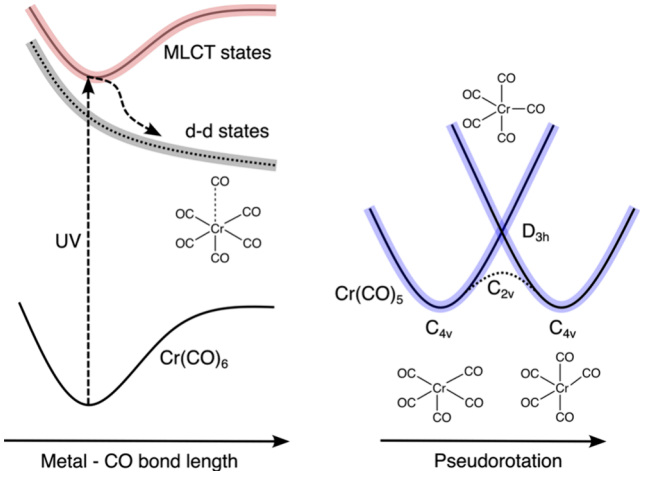

We measure a dephasing time of 830 ± 50 fs for the coherent oscillations observed here, in excellent agreement with the value of 815 ± 20 fs measured in the gas phase.[65] The matching oscillation frequencies and dephasing times clearly indicate that the same equatorial Cr-CO bending modes of $Cr(CO)_5$ are populated in solution and in the gas phase. In solution, and in cases where $Cr(CO)_5$ does not undergo geminate recombination, our findings thus suggest that the octane solvent has no measurable influence on the nature of the initial wavepacket dynamics along the dissociation pathway, nor does the solvent seem to influence the dephasing time of the oscillations. As in the gas phase, we think, the excess vibrational energy is first dissipated via intramolecular vibrational energy redistribution (IVR) to lower-energy modes of the solute. However, the solvent must already provide a bath for energy dissipation within the first picoseconds because, unlike in the gas phase,[65,67] additional ligand dissociation is not observed in solution. It is thus conceivable that the time constant of 8.2 ps, which we assign to the formation of the $Cr(CO)_5$-alkane σ-complex, includes a component that corresponds to a further thermalization of the bare $Cr(CO)_5$

https://doi.org/10.1021/jacs.4c02077
J. Am. Chem. Soc. 2024, 146, 14000−14011

with the solvent environment and that thermalization and alkane association are concerted processes.

It is noteworthy that the coherent oscillations we observe appear in the far-red part of the transient absorption spectrum. Previous flash photolysis experiments of $Cr(CO)_5$ in a neon matrix[13] as well as in perfluorocyclohexane solution[14] observed the fingerprint HOMO → LUMO absorption band in the range of 620 to 630 nm. Because neon and perfluorocyclohexane have been considered to be noninteracting moieties, this has been interpreted to be the signature of bare $Cr(CO)_5$. The absorption spectrum at 0.5 ps in Figure 1b exhibits an absorption band at even higher wavelengths at around 670 nm, which indicates that even neon and perfluorocyclohexane weakly bind the undercoordinated metal center and shift the HOMO → LUMO absorption band to higher energy with respect to the band position measured here. Besides this sensitivity to the nature of the moiety bound to the metal center, it has further previously been shown that the energy of the HOMO → LUMO absorption band also depends on structural distortions and the specific symmetry of the $Cr(CO)_5$ fragment.[13,69,70] Both our observations of a transient absorption band in the far-red absorption range and the modulation of the band by the same characteristic oscillations as in the gas phase therefore strongly point to the formation of bare $Cr(CO)_5$ in solution.

As we show in the following, the purely experimental assignments of the transient optical absorption bands to specific species are confirmed by calculated spectra. Figure 3a contains the experimental steady-state absorption spectrum of $Cr(CO)_6$ as well as transient absorption spectra of bare $Cr(CO)_5$ (delay of 0.5 ps) and the $Cr(CO)_5$-alkane σ-complex (delay of 300 ps). Our simulated spectra of $Cr(CO)_6$, $Cr(CO)_5$, and the $Cr(CO)_5$-octane σ-complex calculated at the TD-DFT level of theory are shown in Figure 3b. Confirming our experimental assignments, the long-lived transient band at 510 nm can be identified with theory as the fingerprint of the $Cr(CO)_5$-alkane σ-complex. Bare $Cr(CO)_5$ in its C_{4v} ground-state geometry instead exhibits an absorption band centered at ∼670 nm. Our calculations also indicate a strong sensitivity of the position of the $Cr(CO)_5$ HOMO → LUMO absorption band to structural distortions. A shift from 670 to 800 nm is calculated when going from the C_{4v} ground-state geometry of $Cr(CO)_5$ to a C_{2v} distorted structure. This distorted structure can be thought to represent a prevalent structure of vibrationally excited $Cr(CO)_5$ where Cr−CO bonds are bent toward the C_{2v} geometry of the transition state along the pseudorotation coordinate[68] (compare Scheme 2). In our calculations, the structure was generated by a restricted optimization of $Cr(CO)_5$ in C_{2v} symmetry, where two opposing equatorial CO groups are bent out of plane by a fixed angle of 15°. An oscillatory motion in $Cr(CO)_5$ between C_{4v} and C_{2v} symmetry along the bending mode of the equatorial CO ligands would thus modulate the intensity in the optical absorption spectrum around 670 nm as observed experimentally. This explains the coherent oscillations on sub-picosecond time scales in this spectral region (see Figure 1a).

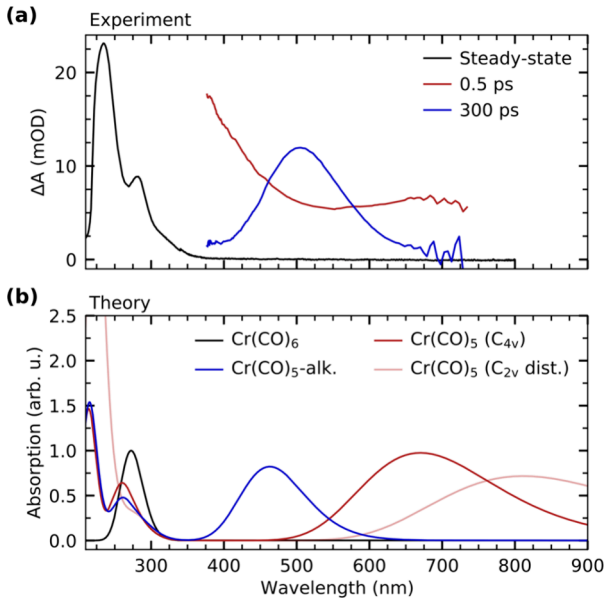

Figure 3. (a) Steady-state optical absorption spectrum of $Cr(CO)_6$ compared with transient optical absorption spectra at 0.5 and 300 ps pump−probe delay. For comparison, the steady-state spectrum is scaled. (b) Calculated absorption spectra of $Cr(CO)_6$, $Cr(CO)_5$ in C_{4v} and a C_{2v} distorted symmetry, and the $Cr(CO)_5$-alkane σ-complex at the TD-DFT level of theory. The calculated spectrum of $Cr(CO)_6$ is scaled so that the transition at ∼290 nm is 1. All other species are scaled accordingly.

We note that the strong absorption band observed during the first picoseconds below 450 nm (see Figure 1a) is not reproduced by theory for any of the calculated species. Still, since the band decays with a time constant of 8.2 ps as the final $Cr(CO)_5$-alkane product rises, we can tentatively attribute the absorption band below 450 nm to a transition of bare $Cr(CO)_5$. During the first picoseconds, bare $Cr(CO)_5$ can be expected to be structurally far from thermal equilibrium. The associated vibrational excitations may then allow the nominally symmetry-forbidden absorption below 450 nm to adopt its substantial oscillator strength. This effect, however, is not reproduced by our level of theory, which is based on vibrational and electronic ground states. Our assignment of the absorption band below 450 nm to bare $Cr(CO)_5$ is corroborated in addition by assessing the residuals of the delay trace at 390 nm (see Figure S1 in the Supporting Information). The delay trace at that wavelength exhibits the same, albeit less pronounced, characteristic oscillations within the first picosecond as the trace at 670 nm, which we identified as one of the fingerprints of the bare $Cr(CO)_5$ intermediate. This assignment of the band below 450 nm is also consistent with its initial intensity decrease with a time constant of 150 fs. The magnitude of the decrease is ∼30%, which is in good agreement with the previously determined yield for a geminate recombination of 34% for $Cr(CO)_5$ in alkane solution.[71]

Our experimental data therefore allow to robustly establish the ultrafast pathway leading to the formation of the $Cr(CO)_5$-alkane σ-complex in octane solution (see Scheme 3): As in the gas phase, CO dissociation and formation of $Cr(CO)_5$ occur on a time scale below 100 fs[65−67] and thus within the time resolution of the experiment here. With a time constant of 150 fs, a fraction of bare $Cr(CO)_5$ molecules undergoes geminate recombination with CO groups, which have not escaped the first solvation shell following dissociation. Those $Cr(CO)_5$ molecules that do not geminately recombine clearly occur in their electronic ground state in C_{4v} symmetry with characteristic equatorial Cr-CO bending modes, which dephase with a time constant of 830 fs. The $Cr(CO)_5$-alkane σ-complex then forms with a time constant of 8.2 ps via a ground-state

https://doi.org/10.1021/jacs.4c02077
J. Am. Chem. Soc. 2024, 146, 14000−14011

Scheme 3. Determined Photochemical Pathway and Associated Time Scales of Alkane σ-Complex Formation Following CO Dissociation from $Cr(CO)_6$ in Octane Solution

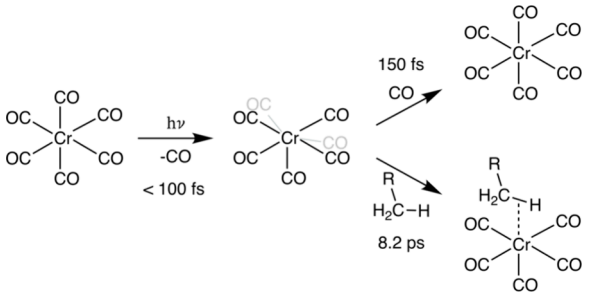

reaction, in which an octane molecule binds to the bare $Cr(CO)_5$. With a time constant of 53 ps, the $Cr(CO)_5$-alkane σ-complex vibrationally cools and persists thereafter.

Time-Resolved X-ray Absorption Spectroscopy. Figure 4a and b show the steady-state X-ray absorption spectra of

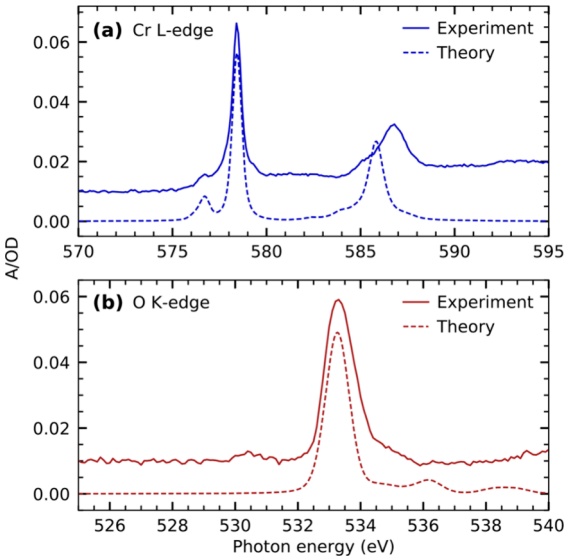

Figure 4. Steady-state X-ray absorption spectra of $Cr(CO)_6$ in octane solution measured at the (a) Cr L-edge and (b) O K-edge compared with calculated spectra at the RASSCF and TD-DFT level of theory, respectively.

$Cr(CO)_6$ in octane solution measured at the Cr L-edge and O K-edge, respectively. The shapes of both spectra are in good agreement with previous soft X-ray absorption measurements on $Cr(CO)_6$ in 1-pentanol solution.[72] Below the measurements, spectra calculated at the RASSCF level of theory are shown for the Cr L-edge as well as the TD-DFT level of theory for the O K-edge. The calculations are in good agreement with experiment and can hence be used to assign the observed spectral features.

The L-edge absorption spectrum of $Cr(CO)_6$ in Figure 4a is split into the L_3- and L_2-edges due to spin−orbit coupling in the core-excited-state final states. The L_3-edge is characterized by two absorption resonances. Based on our calculations, the less intense pre-edge resonance at 576.5 eV can be assigned to excitations of Cr 2p electrons into unoccupied CO π^* orbitals of t_{2g} symmetry. The transitions underlying this resonance carry oscillator strength due to π-backdonation and the associated hybridization of the CO $\pi^*(t_{2g})$ orbitals with the occupied d-derived orbitals of the same symmetry. The stronger main resonance at 578.5 eV is instead due to excitations of Cr 2p electrons into unoccupied 3d-derived orbitals of e_g symmetry. Notably, this ordering of resonances at the metal L-edge is different than in other metal carbonyls of lower symmetry[34,73,74] as well as the isoelectronic ferrous hexacyanide.[75,76] In these complexes, excitations into the unoccupied d levels are at lower energy than excitations into ligand π^* orbitals. This different ordering reflects the higher coordination number in $Cr(CO)_6$ compared to other metal carbonyls as well as, compared to ferrous hexacyanide, the carbonyl group being a stronger π acceptor than the negatively charged cyanide group. Overall, this causes a higher ligand field in $Cr(CO)_6$ and a destabilization of the unoccupied metal d orbitals to higher energies than the ligand π^* orbitals.

The O K-edge spectrum shown in Figure 4b is dominated by a strong absorption resonance at 533.3 eV. Based on our TD-DFT calculations, this resonance can be assigned to excitations of O 1s electrons into the unoccupied CO π^* manifold involving specifically orbitals of t_{1u} and t_{2u} symmetry in agreement with previous studies on solution and gas-phase $Cr(CO)_6$.[72,77,78] The low-intensity prepeak at a photon energy of 530.5 eV is instead tentatively assigned to impurities stemming from the sample preparation. Specifically, based on comparison to previous gas-phase electron energy loss spectroscopy measurements,[77,79,80] the prepeak is most likely due to molecular oxygen dissolved in the octane solution, which was accumulating during the sample preparation (see Methods section).

Figure 5a shows the transient Cr L_3-edge absorption spectra of $Cr(CO)_6$ in octane solution compared with calculated transient spectra as well as with the $Cr(CO)_6$ steady-state spectrum (for comparison, the absolute calculated spectra from which the differences in Figure 5a are generated are shown in Figure 5b). The two experimental difference spectra in Figure 5a were recorded at 90 ps and 50 ns after UV excitation and are identical in shape and intensity. Both spectra exhibit substantial depletion at the energy of the main resonance at 578.4 eV as well as positive transient intensities at 577.9 and 574.9 eV. The delay traces taken at these energies, shown in Figure 5c, are well-described by a step function convolved with a Gaussian function with ∼45 ps fwhm representing the temporal resolution in the X-ray experiments. This is consistent with our transient optical absorption measurements in that the $Cr(CO)_5$-alkane σ-complex is expected to form within the time resolution of the X-ray absorption measurements. Both transient X-ray absorption difference spectra thus constitute the electronic-structure fingerprint of the $Cr(CO)_5$-alkane σ-complex.

This is again consistent with our calculated Cr L_3-edge difference spectra of bare $Cr(CO)_5$ and the $Cr(CO)_5$-alkane σ-complex in Figure 5a. While both calculated difference spectra reproduce the experimentally observed depletion at 578.4 eV and the positive intensity around 577.9 eV, only one of the calculated spectra reproduces the energy of the transient pre-edge peak seen in experiment at 574.9 eV (see inset in Figure 5b). The peak at 574.9 eV is well reproduced by the calculated spectrum of the $Cr(CO)_5$-alkane σ-complex, whereas the bare $Cr(CO)_5$ fragment has a peak at ∼1 eV lower incidence photon energy. The calculated spectrum of the $Cr(CO)_5$-alkane σ-complex additionally shows better agreement in terms of spectral shape around 577.5 eV.

https://doi.org/10.1021/jacs.4c02077
J. Am. Chem. Soc. 2024, 146, 14000−14011

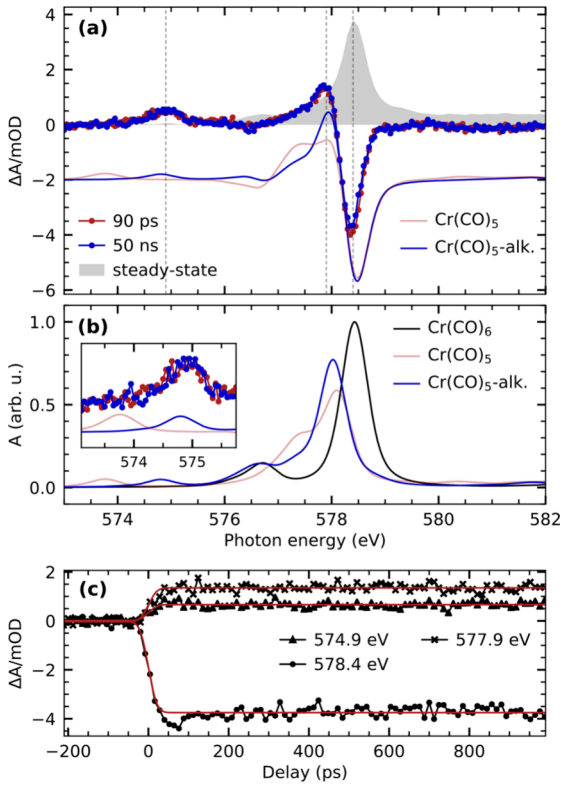

Figure 5. (a) Experimental and calculated transient Cr L_3-edge absorption difference spectra of $Cr(CO)_6$ in octane solution. Calculations are performed at the RASSCF level of theory. Difference spectra of the $Cr(CO)_5$-alkane σ-complex and the $Cr(CO)_5$ fragment are generated with respect to $Cr(CO)_6$ (spectrum of the respective species minus spectrum of $Cr(CO)_6$). For better comparison, the depletion of the calculated $Cr(CO)_5$-alkane difference spectra is scaled to match the depletion of the experimental spectrum, and the $Cr(CO)_5$ difference spectrum is scaled accordingly. The experimental steady-state spectrum is additionally shown for comparison and scaled to match the amplitude of the depletion of the transient difference spectra. (b) Calculated L_3-edge absorption spectrum of $Cr(CO)_6$, the $Cr(CO)_5$-alkane σ-complex, and the $Cr(CO)_5$ fragment. The maximum of the $Cr(CO)_6$ spectrum is scaled to 1, and the other spectra are scaled accordingly. The inset shows a close-up of the transient pre-edge region between 573.1 and 575.75 eV. (c) Pump–probe delay traces measured at the energies indicated in (a). The delay traces are modeled with a step function broadened by a Gaussian function.

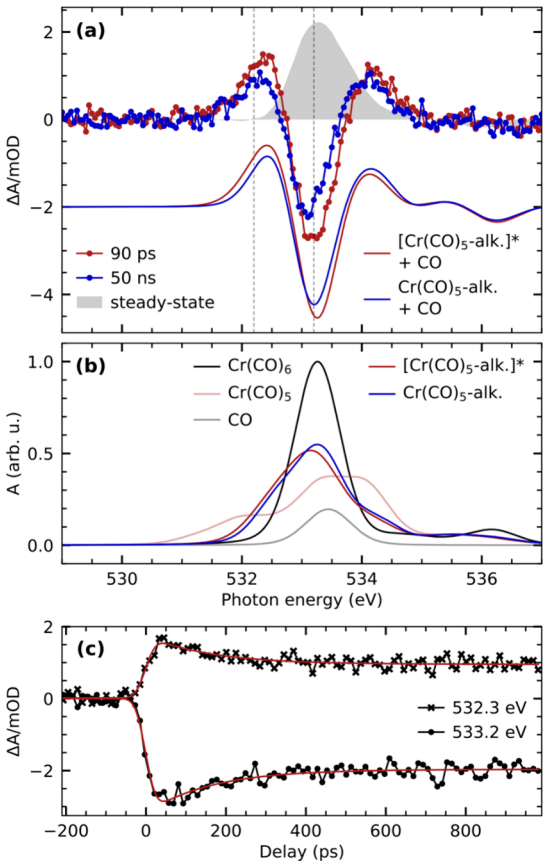

Figure 6. (a) Transient O K-edge absorption difference spectra of $Cr(CO)_6$ in octane solution compared with calculated difference spectra of the $Cr(CO)_5$-alkane σ-complex and the free CO as well as the $Cr(CO)_5$ fragment and the free CO with respect to the $Cr(CO)_6$ species. The depletion of the calculated difference spectrum, which represents the sum of the $Cr(CO)_5$-alkane σ-complex and the free CO, is scaled to match the depletion of the experimental spectrum at 50 ns. The calculated difference spectrum of the "hot" [$Cr(CO)_5$-alkane]* σ-complex plus the free CO is scaled accordingly. The generation of the "hot" [$Cr(CO)_5$-alkane]* σ-complex spectrum is discussed in the main text. The experimental steady-state spectrum is additionally shown for comparison and scaled to match the amplitude of the depletion of the transient difference spectrum at 50 ns. (b) Calculated O K-edge absorption spectra of all species considered in generating the difference spectra displayed in (a). The maximum of the $Cr(CO)_6$ spectrum is scaled to 1. All other spectra are scaled accordingly. (c) Pump–probe delay traces measured at the energies indicated in (a). The delay traces are modeled with a single-exponential decay of a primary species to a stable product.

Measured O K-edge steady-state and transient difference spectra of $Cr(CO)_6$ in octane solution are compared with calculated difference spectra in Figure 6a (absolute calculated spectra are shown in Figure 6b). The two experimental difference spectra (recorded at the same pump–probe delays as at the Cr L_3-edge) exhibit substantial depletion of the main steady-state absorption resonance at 533.2 eV as well as induced absorption in the pre- and postedge region at 532.3 and 534.2 eV. In contrast to the Cr L_3-edge difference spectra, however, the amplitudes of the transient difference spectra change as a function of pump–probe delay. The delay traces measured at the transient pre-edge at 532.2 eV as well as the depletion at 533.2 eV are displayed in Figure 6c. Their temporal evolutions are well-described by single-exponential decays with a common time constant of 160 ± 20 ps of a primary species to a secondary metastable species.

The observed signatures are similar to transient O K-edge signatures measured for the photochemistry of $Cr(CO)_6$ in 1-pentanol solution. There, the observed absorption differences were assigned to the migration dynamics of C–H to O–H coordination toward the $Cr(CO)_5$ species.[72] In the absence of any functional groups besides C–H bonds in the alkane solution, the here-observed signal changes are instead assigned to the decay of high-frequency CO stretching modes of the σ-complex. These modes have previously been shown to be excited following ligand exchange in $Cr(CO)_6$ in alkane solutions.[25,64,81] The vibrational excitations have been reported to only weakly couple to lower-energy vibrations and to relax on a time scale of 160 ps, in excellent agreement with our measurements.

https://doi.org/10.1021/jacs.4c02077
J. Am. Chem. Soc. 2024, 146, 14000–14011

The comparison of the experimental and theoretical difference spectra in Figure 6a explains how these vibrational excitations are reflected in the O K-edge absorption spectra. The spectrum at 50 ns corresponds to the $Cr(CO)_5$-alkane σ-complex plus the dissociated CO ligand. At this delay time, the complex can be safely assumed to be vibrationally cold. At 90 ps instead, the agreement of the calculated spectrum of a "hot" $Cr(CO)_5$-alkane σ-complex with experiment at the pre-edge at 532.3 eV as well as at the main-edge at 533.2 eV suggests that the σ-complex is still vibrationally excited. To reflect vibrational excitations in the calculated spectrum, we empirically added a red-shift of 0.1 eV to the incident photon energy of the cold $Cr(CO)_5$-alkane σ-complex spectrum. The rationale is that excitation of the CO stretching mode leads to a higher average CO bond length, which stabilizes the CO π^* orbitals and shifts O 1s → CO π^* resonances to lower energies. We also added an additional 0.1 eV Gaussian broadening to the "hot" $Cr(CO)_5$-alkane σ-complex spectrum (in addition to the broadening applied to the spectra of vibrationally cold species, see Computational Details) to reflect the higher degree of conformational motion as a result of the vibrational excitation.[82]

Probing the Orbital Correlation Diagram. The combination of time-resolved optical and X-ray absorption spectroscopy at the Cr L-edge and O K-edge allows following the evolution of unoccupied valence orbitals upon CO dissociation and alkane σ-complex formation from three different perspectives. A schematic summary of the evolution of the energies of the decisive valence orbitals and how they are accessed by the three different absorption spectroscopy methods is shown in Scheme 4 (a comprehensive orbital correlation diagram of all valence orbitals included in the active space of the RASSCF calculations is shown in Figure S2 in the Supporting Information).

Scheme 4. Orbital Correlation Diagram along CO Dissociation from $Cr(CO)_6$ to $Cr(CO)_5$ and σ-Complex Formation to $Cr(CO)_5$-Alkane with Main Optical (Gray), O K-Edge (Red), and Cr L-Edge Absorption Transitions (Blue)

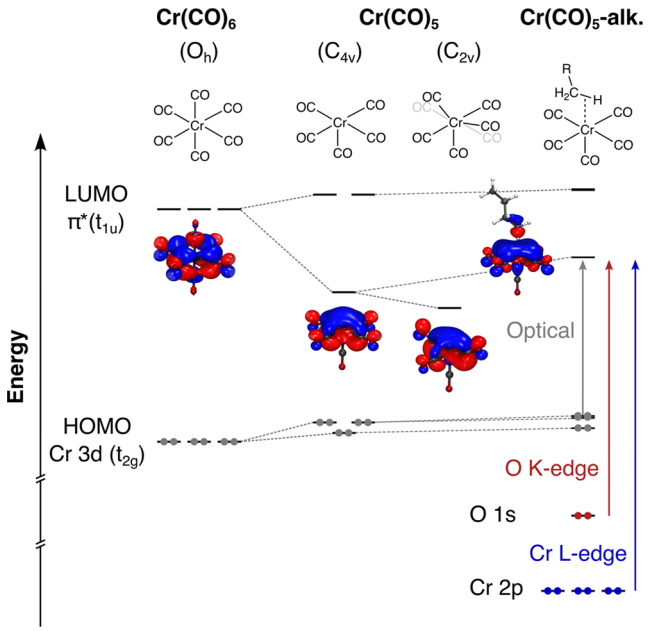

CO dissociation from $Cr(CO)_6$ is initially triggered by a HOMO → LUMO metal-to-ligand charge transfer (MLCT) excitation involving Cr 3d (t_{2g}) → CO π^* (t_{1u}) transitions with an absorption band centered at around 290 nm (see Figure 3). CO dissociation breaks the O_h symmetry and is predominantly reflected in a major decrease of energy of one of the former CO π^* (t_{1u}) orbitals in the $Cr(CO)_5$ fragment (see Scheme 4). Since the HOMOs remain relatively stable, the LUMO energy drop can be experimentally observed in the time-resolved optical absorption data (see Figure 3). The structural changes associated with the coherent oscillation of the Cr-CO bending mode further decrease the energy of the LUMO as our calculations suggest and in agreement with experiment (see Scheme 4). Distortion from C_{4v} to C_{2v} moves two equatorial CO groups out of plane, which reduces hybridization of the nominal CO π^* orbital with the Cr d_{z^2} orbital (see orbital plots in Scheme 4).[68] This change in orbital overlap stabilizes the LUMO and causes the observed red-shift of the HOMO → LUMO absorption band in C_{2v} distorted structures (Figure 3). In the $Cr(CO)_5$-alkane σ-complex, the bonding interactions between the Cr and the C−H bond increase the LUMO energy, as observed in the blue-shift of the HOMO → LUMO absorption band back to higher energies in the optical absorption spectrum (see Scheme 4 and Figure 3). The degree to which the band shifts thus serves as an experimental measure of the strength of the metal−alkane bonding interaction and is mirrored in the time-resolved X-ray absorption spectra.

Following CO dissociation and alkane association, the LUMO remains an orbital of predominantly CO π^* character. It does, however, also adopt some degree of Cr d_{z^2} character due to the discussed changes in Cr-CO hybridization. This emergence of Cr d_{z^2} character is seen in the increase of orbital amplitude of the LUMO at the Cr center when going from $Cr(CO)_6$ to the two $Cr(CO)_5$ geometries and the $Cr(CO)_5$-alkane σ-complex (Scheme 4). By d_{z^2} admixture, the LUMO becomes accessible in Cr L-edge absorption via dipole-allowed 2p → 3d transitions, which can be experimentally observed via the pre-edge peak at 574.9 eV in the transient L_3-edge spectrum of the $Cr(CO)_5$-alkane σ-complex (Figure 5a). Notably, while the transient $Cr(CO)_5$ fragment cannot be observed with picosecond X-ray absorption spectroscopy, the calculated shift of the Cr L-edge pre-edge peak of ~1 eV in the $Cr(CO)_5$-alkane σ-complex to higher energy with respect to bare $Cr(CO)_5$ mirrors the behavior of the optical absorption. In terms of X-ray versus optical absorption, this shift provides a complementary measure of the strength of the metal−alkane bond.

In terms of the ligand versus metal perspective, the predominant ligand character of the LUMO can be accessed with O K-edge absorption spectroscopy in yet another complementary way. In contrast to the Cr L_3-edge, the O K-edge probes the LUMO through dipole-allowed transitions of O 1s electrons into the CO π^* orbitals, which have substantial O 2p character. The LUMO of the $Cr(CO)_5$-alkane σ-complex is observed as a transient pre-edge transition at 532.3 eV (Figure 6a). As in the Cr L_3-edge, a shift of the pre-edge between the $Cr(CO)_5$-alkane σ-complex and the bare $Cr(CO)_5$ fragment can be seen (Figure 6b), again reflecting the relative shift in LUMO energy as a result of alkane binding in the $Cr(CO)_5$-alkane σ-complex (Scheme 4).

Besides providing complementary insights into the evolution of the LUMO along the photochemical pathway, the time-

https://doi.org/10.1021/jacs.4c02077
J. Am. Chem. Soc. 2024, 146, 14000−14011

resolved X-ray absorption data at the Cr L_3-edge and O K-edge further inform on the evolution of the full manifold of unoccupied Cr 3d and ligand CO π^* orbitals, respectively (see Supporting Information for full orbital correlation diagram). The absence of depletion at 576.7 eV in the measured $Cr(CO)_5$-alkane σ-complex spectrum, a region of 2p→ CO $\pi^*(t_{2g})$ transitions (Figure 5a), points to the low impact the ligand exchange has on the t_{2g} manifold. Both the $Cr(CO)_5$-alkane σ-complex and $Cr(CO)_6$ exhibit a similarly intense resonance at the same energy (see Figure 5b), reflecting the unchanged energies of the CO $\pi^*(t_{2g})$ orbitals as well as their unchanged hybridization with Cr 3d orbitals in both species. The Cr L_3-edge spectrum of the $Cr(CO)_5$-alkane σ-complex further reflects the splitting of the $3d(e_g)$ orbitals as a result of the breaking of O_h symmetry upon ligand exchange. This can be seen by the splitting of the main-edge resonance in the calculated $Cr(CO)_5$-alkane σ-complex spectrum, which, in addition to the main maximum at 578 eV, exhibits a shoulder at 577.2 eV (see Figure 5b). In experiment, this splitting is visible by the extension of the positive transient intensity in Figure 5a around 577.3 eV in addition to the peak centered at 577.8 eV. Intensity in this range is attributed to excitations of Cr 2p electrons into predominantly the d_{z^2} orbital, whereas the main maximum reflects excitations predominantly into the $d_{x^2-y^2}$ orbital. Both sets of transitions carry less oscillator strength compared to the main resonance in $Cr(CO)_6$. This difference is due to the hybridization of CO π^* orbitals with the d_{z^2} and $d_{x^2-y^2}$ orbitals in the $Cr(CO)_5$-alkane σ-complex, mixing that is allowed in the broken symmetry of $Cr(CO)_5$-alkane and forbidden in the O_h symmetry of $Cr(CO)_6$. This effect of symmetry breaking is mirrored in the t_{2u} manifold of the CO π^* orbitals. Two t_{2u} orbitals of $Cr(CO)_6$ are destabilized following ligand exchange (Scheme 4), explaining the induced absorption at 534.2 eV in the O K-edge spectrum of the $Cr(CO)_5$-alkane σ-complex (Figure 6a and b).

CONCLUSION

We have used a combination of femtosecond optical absorption spectroscopy and picosecond X-ray absorption spectroscopy at the metal L-edge and ligand K-edge to probe the photochemistry and electronic structure evolution of $Cr(CO)_6$ in octane solution. The femtosecond optical absorption data allowed unequivocally establishing the photochemical pathway of alkane σ-complex formation from $Cr(CO)_6$. Bare $Cr(CO)_5$ was found to form within the time resolution of the experiment followed either by geminate recombination with a time constant of 150 fs or octane association to form the $Cr(CO)_5$-alkane σ-complex with a time constant of 8.2 ps. Preceding σ-complex formation, the $Cr(CO)_5$ fragments, which do not recombine, exhibit coherent oscillations in the optical absorption data. Their frequency and dephasing time are characteristic of equatorial Cr-CO bending modes in the ground state of $Cr(CO)_5$, as shown in comparison to the CO dissociation dynamics of gas-phase $Cr(CO)_6$. With the robustly established photochemical pathways based on the optical absorption data, we then used X-ray absorption spectroscopy to characterize the electronic structure of the $Cr(CO)_5$-alkane σ-complex. The ligand exchange breaks the octahedral symmetry, leading to a rehybridization between metal and ligand orbitals.

We show that substantial shifts of the LUMO energy correlate with several complementary experimental observables and characteristically reflect formation of the undercoordinated metal complex, its structural relaxation to the electronic ground state, and alkane association in a σ-complex. Specifically, the shift in LUMO energy is identified as a novel experiment-based descriptor of the impact of metal−alkane bond formation on the electronic structure in the undercoordinated metal complex. Both time-resolved optical and X-ray absorption spectroscopy can thus be generally established as sensitive probes of the strength associated with the metal−alkane interactions in σ-complexes. This approach can now generally be applied to other σ-complexes to provide a detailed understanding of how varying the stability of metal−alkane bonds in σ-complexes—by choice of metal element and ligand structure—modulates reactivity of σ-complexes. We anticipate future studies, using the orbital-based descriptor of metal−alkane bonding derived here, for precise determination of the mechanistic roles of σ-complexes and their precursors in C−H activation reactions.

ASSOCIATED CONTENT

Supporting Information

The Supporting Information is available free of charge at https://pubs.acs.org/doi/10.1021/jacs.4c02077.

Description of the global fit model; comparison of the residuals of the delay traces at 390 and 670 nm; extended discussion of the origin of the oscillatory signal; details on the line shape model; DFT orbital energies; Cartesian coordinates of the DFT-optimized structures; example input files for the DFT and RASSCF calculations (PDF)

AUTHOR INFORMATION

Corresponding Authors

Raphael M. Jay − *Department of Physics and Astronomy, Uppsala University, 75120 Uppsala, Sweden;* orcid.org/0000-0001-9607-8264; Email: raphael.jay@physics.uu.se

Michael Odelius − *Department of Physics, AlbaNova University Center, Stockholm University, 10691 Stockholm, Sweden;* orcid.org/0000-0002-7023-2486; Email: odelius@fysik.su.se

Nils Huse − *Center for Free-Electron Laser Science, Department of Physics, University of Hamburg, 22761 Hamburg, Germany;* orcid.org/0000-0002-3281-7600; Email: nils.huse@uni-hamburg.de

Philippe Wernet − *Department of Physics and Astronomy, Uppsala University, 75120 Uppsala, Sweden;* orcid.org/0000-0001-7011-9072; Email: philippe.wernet@physics.uu.se

Authors

Michael R. Coates − *Department of Physics, AlbaNova University Center, Stockholm University, 10691 Stockholm, Sweden;* orcid.org/0000-0001-6908-5434

Huan Zhao − *Center for Free-Electron Laser Science, Department of Physics, University of Hamburg, 22761 Hamburg, Germany*

Marc-Oliver Winghart − *Max Born Institute for Nonlinear Optics and Short Pulse Spectroscopy, 12489 Berlin, Germany*

Peng Han − *Max Born Institute for Nonlinear Optics and Short Pulse Spectroscopy, 12489 Berlin, Germany*

Ru-Pan Wang − *Center for Free-Electron Laser Science, Department of Physics, University of Hamburg, 22761 Hamburg, Germany;* Present Address: Deutsches

Elektronen-Synchrotron DESY, 22607 Hamburg, Germany

Jessica Harich − *Center for Free-Electron Laser Science, Department of Physics, University of Hamburg, 22761 Hamburg, Germany*

Ambar Banerjee − *Department of Physics and Astronomy, Uppsala University, 75120 Uppsala, Sweden;* Present Address: Research Institute for Sustainable Energy (RISE), TCG Centres for Research and Education in Science and Technology (TCG-CREST), Kolkata 700091, India

Hampus Wikmark − *Department of Physics and Astronomy, Uppsala University, 75120 Uppsala, Sweden;* Present Address: Proximion AB, 164 40 Kista, Sweden

Mattis Fondell − *Institute for Methods and Instrumentation for Synchrotron Radiation Research, Helmholtz-Zentrum Berlin für Materialien und Energie GmbH, 12489 Berlin, Germany*

Erik T. J. Nibbering − *Max Born Institute for Nonlinear Optics and Short Pulse Spectroscopy, 12489 Berlin, Germany;* orcid.org/0000-0001-5874-8052

Complete contact information is available at: https://pubs.acs.org/10.1021/jacs.4c02077

Notes

The authors declare no competing financial interest.

■ ACKNOWLEDGMENTS

We thank the Helmholtz-Zentrum Berlin für Materialien und Energie GmbH for the allocation of synchrotron radiation beamtime. The computations were partly enabled by resources provided by the Swedish National Infrastructure for Computing (SNIC) at UPPMAX, which is partially funded by the Swedish Research Council through grant agreement nos. 2021-22968 and 2022-22975. The computations were also partly enabled by resources provided by the National Academic Infrastructure for Supercomputing in Sweden (NAISS) and the SNIC at the National Supercomputer Centre in Sweden (NSC) and the PDC (Parallelldatorcentrum) Center for High Performance Computing, which are partially funded by the Swedish Research Council through grant agreement nos. 2022-06725 and 2018-05973. A.B. and P.W. acknowledge funding from the Carl Tryggers Foundation (contract CTS 19:399). P.W. acknowledges funding from the Swedish Research Council (grant agreement no. 2019-04796). H.Z., J.H., and N.H. acknowledge funding from the Cluster of Excellence "CUI: Advanced Imaging of Matter" of the German Research Association (DFG), EXC 2056, project ID 390715994. R.-P.W. acknowledges funding from the German Ministry of Education and Research (BMBF), project ID 05K19GU2. M.O. acknowledges funding from Swedish Research Council grant agreement no. 2021-04521. M.-O.W., P.H., and E.T.J.N. acknowledge funding by the European Research Council (ERC) under the European Union's Horizon 2020 research and innovation program (ERC grant agreement no. 788704, E.T.J.N.).

■ REFERENCES

(1) Bergman, R. G. C−H Activation. *Nature* **2007**, *446* (7134), 391−393.

(2) Labinger, J. A.; Bercaw, J. E. Understanding and Exploiting C−H Bond Activation. *Nature* **2002**, *417* (6888), 507−514.

(3) Weller, A. S.; Chadwick, F. M.; McKay, A. I. Transition Metal Alkane-Sigma Complexes. In *Advances in Organometallic Chemistry*; Elsevier Inc., 2016; Vol. *66*, pp 223−276.

(4) Altus, K. M.; Love, J. A. The Continuum of Carbon−Hydrogen (C−H) Activation Mechanisms and Terminology. *Commun. Chem.* **2021**, *4* (1), 173.

(5) Perutz, R. N.; Torres, O.; Vlček, A. Photochemistry of Metal Carbonyls. In *Comprehensive Inorganic Chemistry II*; Elsevier, 2013; pp 229−253.

(6) Hall, C.; Perutz, R. N. Transition Metal Alkane Complexes †. *Chem. Rev.* **1996**, *96* (8), 3125−3146.

(7) Cowan, A.; George, M. Formation and Reactivity of Organometallic Alkane Complexes. *Coord. Chem. Rev.* **2008**, *252* (23−24), 2504−2511.

(8) Pike, S. D.; Thompson, A. L.; Algarra, A. G.; Apperley, D. C.; Macgregor, S. A.; Weller, A. S. Synthesis and Characterization of a Rhodium(I) σ-Alkane Complex in the Solid State. *Science* **2012**, *337* (6102), 1648−1651.

(9) Chadwick, F. M.; Krämer, T.; Gutmann, T.; Rees, N. H.; Thompson, A. L.; Edwards, A. J.; Buntkowsky, G.; Macgregor, S. A.; Weller, A. S. Selective C−H Activation at a Molecular Rhodium Sigma-Alkane Complex by Solid/Gas Single-Crystal to Single-Crystal H/D Exchange. *J. Am. Chem. Soc.* **2016**, *138* (40), 13369−13378.

(10) Bernskoetter, W. H.; Schauer, C. K.; Goldberg, K. I.; Brookhart, M. Characterization of a Rhodium(I) σ-Methane Complex in Solution. *Science* **2009**, *326* (5952), 553−556.

(11) Turner, J. J.; Burdett, J. K.; Perutz, R. N.; Poliakoff, M. Matrix Photochemistry of Metal Carbonyls. *Pure Appl. Chem.* **1977**, *49* (3), 271−285.

(12) Kelly, J. M.; Hermann, H.; von Gustorf, E. K. Observation of Pentacarbonylchromium on Flash Photolysis of Hexacarbonylchromium in Cyclohexane Solution. *J. Chem. Soc. Chem. Commun.* **1973**, No. 4, 105.

(13) Perutz, R. N.; Turner, J. J. Photochemistry of the Group 6 Hexacarbonyls in Low-Temperature Matrices. III. Interaction of the Pentacarbonyls with Noble Gases and Other Matrices. *J. Am. Chem. Soc.* **1975**, *97* (17), 4791−4800.

(14) Bonneau, R.; Kelly, J. M. Flash Photolysis of Chromium Hexacarbonyl in Perfluorocarbon Solvents. Observation of a Highly Reactive Chromium Pentacarbonyl. *J. Am. Chem. Soc.* **1980**, *102* (3), 1220−1221.

(15) Ball, G. E.; Brookes, C. M.; Cowan, A. J.; Darwish, T. A.; George, M. W.; Kawanami, H. K.; Portius, P.; Rourke, J. P. A Delicate Balance of Complexation vs. Activation of Alkanes Interacting with $[Re(Cp)(CO)(PF_3)]$ Studied with NMR and Time-Resolved IR Spectroscopy. *Proc. Natl. Acad. Sci. U. S. A.* **2007**, *104* (17), 6927−6932.

(16) Bromberg, S. E.; Yang, H.; Asplund, M. C.; Lian, T.; McNamara, B. K.; Kotz, K. T.; Yeston, J. S.; Wilkens, M.; Frei, H.; Bergman, R. G.; Harris, C. B. The Mechanism of a C-H Bond Activation Reaction in Room-Temperature Alkane Solution. *Science* **1997**, *278* (5336), 260−263.

(17) George, M. W.; Hall, M. B.; Jina, O. S.; Portius, P.; Sun, X.-Z.; Towrie, M.; Wu, H.; Yang, X.; Zaric, S. D. Understanding the Factors Affecting the Activation of Alkane by $Cp'Rh(CO)_2$ (Cp' = Cp or Cp*). *Proc. Natl. Acad. Sci. U. S. A.* **2010**, *107* (47), 20178−20183.

(18) Lawes, D. J.; Geftakis, S.; Ball, G. E. Insight into Binding of Alkanes to Transition Metals from NMR Spectroscopy of Isomeric Pentane and Isotopically Labeled Alkane Complexes. *J. Am. Chem. Soc.* **2005**, *127* (12), 4134−4135.

(19) Pitts, A. L.; Wriglesworth, A.; Sun, X. Z.; Calladine, J. A.; Zarić, S. D.; George, M. W.; Hall, M. B. Carbon-Hydrogen Activation of Cycloalkanes by Cyclopentadienylcarbonylrhodium-A Lifetime Enigma. *J. Am. Chem. Soc.* **2014**, *136* (24), 8614−8625.

(20) Watson, J. D.; Field, L. D.; Ball, G. E. Binding Methane to a Metal Centre. *Nat. Chem.* **2022**, *14* (7), 801−804.

(21) Aucott, B. J.; Duhme-Klair, A.-K.; Moulton, B. E.; Clark, I. P.; Sazanovich, I. V.; Towrie, M.; Hammarback, L. A.; Fairlamb, I. J. S.; Lynam, J. M. Manganese Carbonyl Compounds Reveal Ultrafast

Metal−Solvent Interactions. *Organometallics* **2019**, *38* (11), 2391−2401.
(22) Shanoski, J. E.; Glascoe, E. A.; Harris, C. B. Ligand Rearrangement Reactions of $Cr(CO)_6$ in Alcohol Solutions: Experiment and Theory. *J. Phys. Chem. B* **2006**, *110* (2), 996−1005.
(23) Sension, R. J.; McClain, T. P.; Lamb, R. M.; Alonso-Mori, R.; Lima, F. A.; Ardana-Lamas, F.; Biednov, M.; Chollet, M.; Chung, T.; Deb, A.; Dewan, P. A.; Gee, L. B.; Huang Ze En, J.; Jiang, Y.; Khakhulin, D.; Li, J.; Michocki, L. B.; Miller, N. A.; Otte, F.; Uemura, Y.; van Driel, T. B.; Penner-Hahn, J. E. Watching Excited State Dynamics with Optical and X-Ray Probes: The Excited State Dynamics of Aquocobalamin and Hydroxocobalamin. *J. Am. Chem. Soc.* **2023**, *145* (25), 14070−14086.
(24) Ryland, E. S.; Lin, M. F.; Verkamp, M. A.; Zhang, K.; Benke, K.; Carlson, M.; Vura-Weis, J. Tabletop Femtosecond M-Edge X-Ray Absorption Near-Edge Structure of FeTPPCl: Metalloporphyrin Photophysics from the Perspective of the Metal. *J. Am. Chem. Soc.* **2018**, *140* (13), 4691−4696.
(25) King, J. C.; Zhang, J. Z.; Schwartz, B. J.; Harris, C. B. Vibrational Relaxation of $M(CO)_6$ (M = Cr, Mo, W): Effect of Metal Mass on Vibrational Cooling Dynamics and Non-Boltzmann Internal Energy Distributions. *J. Chem. Phys.* **1993**, *99* (10), 7595−7601.
(26) Simon, J. D.; Xie, X. Photodissociation of $Cr(CO)_6$ in 1-Propanol and 2-Propanol: Effect of Solvent Structure on the Mechanisms of Formation of $Cr(CO)_5(OHR)$ from Photogenerated $Cr(CO)_5(ROH)$. *J. Phys. Chem.* **1989**, *93* (1), 291−293.
(27) Simon, J. D.; Xie, X. Time-Resolved Studies of Solvation: The Photodissociation of $Cr(CO)_6$ in Pentanol. *J. Phys. Chem.* **1987**, *91* (22), 5538−5540.
(28) Simon, J. D.; Xie, X. Photodissociation of $Cr(CO)_6$ in Solution: Direct Observation of the Formation of $Cr(CO)_5(MeOH)$. *J. Phys. Chem.* **1986**, *90* (26), 6751−6753.
(29) Joly, A. G.; Nelson, K. A. Femtosecond Transient Absorption Spectroscopy of $Cr(CO)_6$ in Methanol: Observation of Initial Excited States and CO Dissociation. *J. Phys. Chem.* **1989**, *93* (8), 2876−2878.
(30) Joly, A. G.; Nelson, K. A. Metal Carbonyl Photochemistry in Organic Solvents: Femtosecond Transient Absorption and Preliminary Resonance Raman Spectroscopy. *Chem. Phys.* **1991**, *152* (1−2), 69−82.
(31) Reinhard, M.; Auböck, G.; Besley, N. A.; Clark, I. P.; Greetham, G. M.; Hanson-Heine, M. W. D.; Horvath, R.; Murphy, T. S.; Penfold, T. J.; Towrie, M.; George, M. W.; Chergui, M. Photoaquation Mechanism of Hexacyanoferrate(II) Ions: Ultrafast 2D UV and Transient Visible and IR Spectroscopies. *J. Am. Chem. Soc.* **2017**, *139* (21), 7335−7347.
(32) Henke, W. C.; Otolski, C. J.; Moore, W. N. G.; Elles, C. G.; Blakemore, J. D. Ultrafast Spectroscopy of $[Mn(CO)_3]$ Complexes: Tuning the Kinetics of Light-Driven CO Release and Solvent Binding. *Inorg. Chem.* **2020**, *59* (4), 2178−2187.
(33) Bartlett, S. A.; Besley, N. A.; Dent, A. J.; Diaz-Moreno, S.; Evans, J.; Hamilton, M. L.; Hanson-Heine, M. W. D.; Horvath, R.; Manici, V.; Sun, X.-Z.; Towrie, M.; Wu, L.; Zhang, X.; George, M. W. Monitoring the Formation and Reactivity of Organometallic Alkane and Fluoroalkane Complexes with Silanes and Xe Using Time-Resolved X-Ray Absorption Fine Structure Spectroscopy. *J. Am. Chem. Soc.* **2019**, *141* (29), 11471−11480.
(34) Jay, R. M.; Banerjee, A.; Leitner, T.; Wang, R.-P.; Harich, J.; Stefanuik, R.; Wikmark, H.; Coates, M. R.; Beale, E. V.; Kabanova, V.; Kahraman, A.; Wach, A.; Ozerov, D.; Arrell, C.; Johnson, P. J. M.; Borca, C. N.; Cirelli, C.; Bacellar, C.; Milne, C.; Huse, N.; Smolentsev, G.; Huthwelker, T.; Odelius, M.; Wernet, P. Tracking C−H Activation with Orbital Resolution. *Science* **2023**, *380* (6648), 955−960.
(35) Cobar, E. A.; Khaliullin, R. Z.; Bergman, R. G.; Head-Gordon, M. Theoretical Study of the Rhenium Alkane Interaction in Transition Metal Alkane-Complexes. *Proc. Natl. Acad. Sci. U. S. A.* **2007**, *104* (17), 6963−6968.
(36) Saillard, J. Y.; Hoffmann, R. Carbon-Hydrogen and Hydrogen-Hydrogen Activation in Transition Metal Complexes and on Surfaces. *J. Am. Chem. Soc.* **1984**, *106* (7), 2006−2026.
(37) Siegbahn, P. E. M.; Svensson, M. Different Electronic Structure Requirements on Precursors and Transition States for the Oxidative Addition Reaction with Methane. *J. Am. Chem. Soc.* **1994**, *116* (22), 10124−10128.
(38) Balcells, D.; Clot, E.; Eisenstein, O. C—H Bond Activation in Transition Metal Species from a Computational Perspective. *Chem. Rev.* **2010**, *110* (2), 749−823.
(39) Miedema, P. S.; Quevedo, W.; Fondell, M. The Variable Polarization Undulator Beamline UE52 SGM at BESSY II. *J. Large-Scale Res. Facil. JLSRF* **2016**, *2*, 2−5.
(40) Ekimova, M.; Quevedo, W.; Faube, M.; Wernet, P.; Nibbering, E. T. J. A Liquid Flatjet System for Solution Phase Soft-x-Ray Spectroscopy. *Struct. Dyn.* **2015**, *2*, No. 054301.
(41) Fondell, M.; Eckert, S.; Jay, R. M.; Weniger, C.; Quevedo, W.; Niskanen, J.; Kennedy, B.; Sorgenfrei, F.; Schick, D.; Giangrisostomi, E.; Ovsyannikov, R.; Adamczyk, K.; Huse, N.; Wernet, P.; Mitzner, R.; Föhlisch, A. Time-Resolved Soft X-Ray Absorption Spectroscopy in Transmission Mode on Liquids at MHz Repetition Rates. *Struct. Dyn.* **2017**, *4* (5), No. 054902.
(42) Henke, B. L.; Gullikson, E. M.; Davis, J. C. X-Ray Interactions: Photoabsorption, Scattering, Transmission, and Reflection at E = 50−30, 000 EV, Z = 1−92. *Atomic Data and Nuclear Data Tables* **1993**, *54*, 181−342.
(43) Frisch, M. J.; Trucks, G. W.; Schlegel, H. B.; Scuseria, G. E.; Robb, M. A.; Cheeseman, J. R.; Scalmani, G.; Barone, V.; Petersson, G. A.; Nakatsuji, H.; Li, X.; Caricato, M.; Marenich, A. V.; Bloino, J.; Janesko, B. G.; Gomperts, R.; Mennucci, B.; Hratchian, H. P.; Ortiz, J. V.; Izmaylov, A. F.; Sonnenberg, J. L.; Williams-Young, D.; Ding, F.; Lipparini, F.; Egidi, F.; Goings, J.; Peng, B.; Petrone, A.; Henderson, T.; Ranasinghe, D.; Zakrzewski, V. G.; Gao, J.; Rega, N.; Zheng, G.; Liang, W.; Hada, M.; Ehara, M.; Toyota, K.; Fukuda, R.; Hasegawa, J.; Ishida, M.; Nakajima, T.; Honda, Y.; Kitao, O.; Nakai, H.; Vreven, T.; Throssell, K.; Montgomery, J. A., Jr.; Peralta, J. E.; Ogliaro, F.; Bearpark, M. J.; Heyd, J. J.; Brothers, E. N.; Kudin, K. N.; Staroverov, V. N.; Keith, T. A.; Kobayashi, R.; Normand, J.; Raghavachari, K.; Rendell, A. P.; Burant, J. C.; Iyengar, S. S.; Tomasi, J.; Cossi, M.; Millam, J. M.; Klene, M.; Adamo, C.; Cammi, R.; Ochterski, J. W.; Martin, R. L.; Morokuma, K.; Farkas, O.; Foresman, J. B.; Fox, D. J. *Gaussian 16*, Revision C.01; Gaussian, Inc.: Wallingford, CT, 2016.
(44) Tao, J.; Perdew, J. P.; Staroverov, V. N.; Scuseria, G. E. Climbing the Density Functional Ladder: Nonempirical Meta−Generalized Gradient Approximation Designed for Molecules and Solids. *Phys. Rev. Lett.* **2003**, *91* (14), No. 146401.
(45) Staroverov, V. N.; Scuseria, G. E.; Tao, J.; Perdew, J. P. Comparative Assessment of a New Nonempirical Density Functional: Molecules and Hydrogen-Bonded Complexes. *J. Chem. Phys.* **2003**, *119* (23), 12129−12137.
(46) Weigend, F.; Ahlrichs, R. Balanced Basis Sets of Split Valence, Triple Zeta Valence and Quadruple Zeta Valence Quality for H to Rn: Design and Assessment of Accuracy. *Phys. Chem. Chem. Phys.* **2005**, *7* (18), 3297−3305.
(47) Weigend, F. Accurate Coulomb-Fitting Basis Sets for H to Rn. *Phys. Chem. Chem. Phys.* **2006**, *8* (9), 1057−1065.
(48) Barone, V.; Cossi, M. Quantum Calculation of Molecular Energies and Energy Gradients in Solution by a Conductor Solvent Model. *J. Phys. Chem. A* **1998**, *102* (11), 1995−2001.
(49) Cossi, M.; Rega, N.; Scalmani, G.; Barone, V. Polarizable Dielectric Model of Solvation with Inclusion of Charge Penetration Effects. *J. Chem. Phys.* **2001**, *114* (13), 5691−5701.
(50) Malmqvist, P. Å.; Rendell, A.; Roos, B. O. The Restricted Active Space Self-Consistent-Field Method, Implemented with a Split Graph Unitary Group Approach. *J. Phys. Chem.* **1990**, *94* (14), 5477−5482.
(51) Aquilante, F.; Autschbach, J.; Baiardi, A.; Battaglia, S.; Borin, V. A.; Chibotaru, L. F.; Conti, I.; De Vico, L.; Delcey, M.; Fdez. Galván, I.; Ferré, N.; Freitag, L.; Garavelli, M.; Gong, X.; Knecht, S.; Larsson,

https://doi.org/10.1021/jacs.4c02077
J. Am. Chem. Soc. 2024, 146, 14000−14011

E. D.; Lindh, R.; Lundberg, M.; Malmqvist, P. Å.; Nenov, A.; Norell, J.; Odelius, M.; Olivucci, M.; Pedersen, T. B.; Pedraza-González, L.; Phung, Q. M.; Pierloot, K.; Reiher, M.; Schapiro, I.; Segarra-Martí, J.; Segatta, F.; Seijo, L.; Sen, S.; Sergentu, D.-C.; Stein, C. J.; Ungur, L.; Vacher, M.; Valentini, A.; Veryazov, V. Modern Quantum Chemistry with [Open]Molcas. *J. Chem. Phys.* **2020**, *152* (21), No. 214117.

(52) Reiher, M.; Salomon, O.; Artur Hess, B. Reparameterization of Hybrid Functionals Based on Energy Differences of States of Different Multiplicity. *Theor. Chem. Accounts Theory, Comput. Model. (Theoretica Chim. Acta)* **2001**, *107* (1), 48−55.

(53) Roos, B. O.; Lindh, R.; Malmqvist, P. Å.; Veryazov, V.; Widmark, P. O. Main Group Atoms and Dimers Studied with a New Relativistic ANO Basis Set. *J. Phys. Chem. A* **2004**, *108* (15), 2851−2858.

(54) Roos, B. O.; Lindh, R.; Malmqvist, P. Å.; Veryazov, V.; Widmark, P. O. New Relativistic ANO Basis Sets for Transition Metal Atoms. *J. Phys. Chem. A* **2005**, *109* (29), 6575−6579.

(55) Malmqvist, P. Å.; Roos, B. O.; Schimmelpfennig, B. The Restricted Active Space (RAS) State Interaction Approach with Spin-Orbit Coupling. *Chem. Phys. Lett.* **2002**, *357* (3−4), 230−240.

(56) Neese, F. Software Update: The ORCA Program System—Version 5.0. *WIREs Comput. Mol. Sci.* **2022**, *12* (5), 1−15.

(57) Neese, F. The ORCA Program System. *Wiley Interdiscip. Rev. Comput. Mol. Sci.* **2012**, *2* (1), 73−78.

(58) Becke, A. D. Density-Functional Exchange-Energy Approximation with Correct Asymptotic Behavior. *Phys. Rev. A* **1988**, *38* (6), 3098−3100.

(59) Becke, A. D. A New Mixing of Hartree-Fock and Local Density-Functional Theories. *J. Chem. Phys.* **1993**, *98* (2), 1372−1377.

(60) Neese, F.; Wennmohs, F.; Hansen, A.; Becker, U. Efficient, Approximate and Parallel Hartree-Fock and Hybrid DFT Calculations. A "chain-of-Spheres" Algorithm for the Hartree-Fock Exchange. *Chem. Phys.* **2009**, *356* (1−3), 98−109.

(61) Pipek, J.; Mezey, P. G. A Fast Intrinsic Localization Procedure Applicable for Ab Initio and Semiempirical Linear Combination of Atomic Orbital Wave Functions. *J. Chem. Phys.* **1989**, *90* (9), 4916−4926.

(62) Campbell, J. L.; Papp, T. Widths of the Atomic K-N7 Levels. *At. Data Nucl. Data Tables* **2001**, *77* (1), 1−56.

(63) Lian, T.; Bromberg, S. E.; Asplund, M. C.; Yang, H.; Harris, C. B. Femtosecond Infrared Studies of the Dissociation and Dynamics of Transition Metal Carbonyls in Solution. *J. Phys. Chem.* **1996**, *100* (29), 11994−12001.

(64) Dougherty, T. P.; Heilweil, E. J. Ultrafast Transient Infrared Absorption Studies of $M(CO)_6$ (M = Cr, Mo or W) Photoproducts in n-Hexane Solution. *Chem. Phys. Lett.* **1994**, *227* (1−2), 19−25.

(65) Trushin, S. A.; Fuss, W.; Schmid, W. E.; Kompa, K. L. Femtosecond Dynamics and Vibrational Coherence in Gas-Phase Ultraviolet Photodecomposition of $Cr(CO)_6$. *J. Phys. Chem. A* **1998**, *102* (23), 4129−4137.

(66) Fuß, W.; Trushin, S. A.; Schmid, W. E. Ultrafast Photochemistry of Metal Carbonyls. *Res. Chem. Intermed.* **2001**, *27* (4−5), 447−457.

(67) Trushin, S. A.; Kosma, K.; Fuß, W.; Schmid, W. E. Wavelength-Independent Ultrafast Dynamics and Coherent Oscillation of a Metal−Carbon Stretch Vibration in Photodissociation of $Cr(CO)_6$ in the Region of 270−345nm. *Chem. Phys.* **2008**, *347* (1−3), 309−323.

(68) Paterson, M. J.; Hunt, P. A.; Robb, M. A.; Takahashi, O. Non-Adiabatic Direct Dynamics Study of Chromium Hexacarbonyl Photodissociation. *J. Phys. Chem. A* **2002**, *106* (44), 10494−10504.

(69) Guenzburger, D.; Caride, A. O.; Zuleta, E. Molecular Orbital Energy Levels in Square-Pyramidal $Co(CN)_5^{3-}$ Ion. *Chem. Phys. Lett.* **1972**, *14* (2), 239−241.

(70) Burdett, J. K. A New Method for the Determination of the Geometries of Binary Transition Metal Complexes. *Inorg. Chem.* **1975**, *14* (2), 375−382.

(71) Wieland, S.; Van Eldik, R. Effect of Solvent and Pressure on the Reactivity of Photoproduced $M(CO)_5$ Transients, as Revealed by the Observed Quantum Yields for the Photosubstitution of $M(CO)_6$ (M = Cr, Mo, W). *J. Phys. Chem.* **1990**, *94* (15), 5865−5870.

(72) Mascarenhas, E. J.; Fondell, M.; Büchner, R.; Eckert, S.; Vaz da Cruz, V.; Föhlisch, A. Photo-Induced Ligand Substitution of $Cr(CO)_6$ in 1-Pentanol Probed by Time Resolved X-Ray Absorption Spectroscopy. *Phys. Chem. Chem. Phys.* **2022**, *24* (30), 17979−17985.

(73) Suljoti, E.; Garcia-Diez, R.; Bokarev, S. I.; Lange, K. M.; Schoch, R.; Dierker, B.; Dantz, M.; Yamamoto, K.; Engel, N.; Atak, K.; Kühn, O.; Bauer, M.; Rubensson, J.-E.; Aziz, E. F. Direct Observation of Molecular Orbital Mixing in a Solvated Organometallic Complex. *Angew. Chemie Int. Ed.* **2013**, *52* (37), 9841−9844.

(74) Wernet, P.; Kunnus, K.; Josefsson, I.; Rajkovic, I.; Quevedo, W.; Beye, M.; Schreck, S.; Grübel, S.; Scholz, M.; Nordlund, D.; Zhang, W.; Hartsock, R. W.; Schlotter, W. F.; Turner, J. J.; Kennedy, B.; Hennies, F.; De Groot, F. M. F.; Gaffney, K. J.; Techert, S.; Odelius, M.; Föhlisch, A. Orbital-Specific Mapping of the Ligand Exchange Dynamics of $Fe(CO)_5$ in Solution. *Nature* **2015**, *520* (7545), 78−81.

(75) Hocking, R. K.; Wasinger, E. C.; De Groot, F. M. F.; Hodgson, K. O.; Hedman, B.; Solomon, E. I. Fe L-Edge XAS Studies of $K_4[Fe(CN)_6]$ and $K_3[Fe(CN)_6]$: A Direct Probe of Back-Bonding. *J. Am. Chem. Soc.* **2006**, *128* (32), 10442−10451.

(76) Kunnus, K.; Zhang, W.; Delcey, M. G.; Pinjari, R. V.; Miedema, P. S.; Schreck, S.; Quevedo, W.; Schröder, H.; Föhlisch, A.; Gaffney, K. J.; Lundberg, M.; Odelius, M.; Wernet, P. Viewing the Valence Electronic Structure of Ferric and Ferrous Hexacyanide in Solution from the Fe and Cyanide Perspectives. *J. Phys. Chem. B* **2016**, *120* (29), 7182−7194.

(77) Cooper, G.; Sze, K. H.; Brion, C. E. Core and Valence-Shell Electronic Excitation of the Group VI Transition-Metal (Chromium, Molybdenum, and Tungsten) Hexacarbonyls by High-Resolution Electron Energy Loss Spectroscopy. *J. Am. Chem. Soc.* **1990**, *112* (11), 4121−4127.

(78) Yang, L.; Ågren, H.; Pettersson, L. G. M.; Guo, J.; Såthe, C.; Föhlisch, A.; Nilsson, A.; Nordgren, J. Core Electron Spectroscopy of Chromium Hexacarbonyl. A Comparative Theoretical and Experimental Study. *Phys. Scr.* **1999**, *59* (2), 138−146.

(79) Hitchcock, A. P.; Wen, A. T.; Ruhl, E. Inner-Shell Electron Energy Loss Spectroscopy of Organometallic Compounds. *J. Electron Spectrosc. Relat. Phenom.* **1990**, *51* (C), 653−660.

(80) Hitchcock, A. P.; Brion, C. E. K-Shell Excitation Spectra of CO, N_2 and O_2. *J. Electron Spectrosc. Relat. Phenom.* **1980**, *18* (1), 1−21.

(81) Yu, S. C.; Xu, X.; Lingle, R.; Hopkins, J. B. The Role of Vibrational Energy in the Ultrafast Photodissociation of Chromium Hexacarbonyl. *J. Am. Chem. Soc.* **1990**, *112* (9), 3668−3669.

(82) Hua, W.; Tian, G.; Fronzoni, G.; Li, X.; Stener, M.; Luo, Y. Fe L-Edge X-Ray Absorption Spectra of Fe(II) Polypyridyl Spin Crossover Complexes from Time-Dependent Density Functional Theory. *J. Phys. Chem. A* **2013**, *117* (51), 14075−14085.

https://doi.org/10.1021/jacs.4c02077
J. Am. Chem. Soc. 2024, 146, 14000−14011